

ASSESSMENT OF NON DIFFRACTIVE CONTRIBUTIONS IN THE FORMATION AND ANALYSIS OF DIGITAL HOLOGRAMS

Fabrice R.A. ONOFRI

¹ Aix-Marseille Université, CNRS, IUSTI, UMR 7343, 13453 Marseille Cedex 13, France

*Corresponding author: fabrice.onofri@univ-amu.fr

Abstract

The influence of non-diffractive scattering mechanisms in the formation and analysis of Digital-In-Line (DIH) holograms is studied. The electromagnetic calculations are performed with the Generalized Lorenz-Mie Theory (GLMT), as well as Debye's series and the localization principle. Numerical results clearly demonstrate the importance to account for partially refracted waves and, to a lesser extend, of edge waves effects.

1 Introduction

DIH is generally considered to be a laser diffraction technique operating in the near-field (i.e. for Fresnel numbers, $F \geq 1$ [1]). As the result of a pure diffraction process, induced by the discontinuity in the optical properties of the propagating medium at the particle boundary (2D projected contour of the particle), the hologram characteristics are thus independent from the particle material properties. Therefore, the hologram formation can be simply modelled with the scalar diffraction theory and a particle model reduced to a two-dimensional opaque disk (or a pinhole, according to Babinet's principle)[1].

However, in the recent years, several groups have demonstrated that with DIH the refractive index of a spherical particle can be measured, with a reasonable accuracy, from the analysis of its hologram. For micron-sized particles, this measure of the refractive index is obtained using a parametric method fitting the particle hologram intensity profile with those calculated with the Lorenz-Mie Theory (LMT, e.g. [2, 3]). For larger particles, the refractive index can be measured directly from the analysing of the relative position of the photonic jet (PJ), also called the focusing or forward caustic region [4-7] produced by rays that are single refracted within the particle [8]. These two approaches clearly infirm the aforementioned vision of hologram formation. To go further on, and most notably to extract more accurate or additional data from particle holograms, it is fundamental to better understand how the particle material properties and the various scattering mechanisms influence the formation of a hologram. This is important whether the particle properties are retrieved from the hologram directly, with a back propagation

method (e.g. [4, 9, 10]), or with an inverse approach (e.g. [11, 12]).

The goal of the present work is precisely to investigate these relative contributions and more specially the non-diffractive scattering mechanisms. The extended abstract is organized as follows. After this brief introduction, section 2 introduces and discusses the basic equations to calculate rigorously, in the frame of the GLMT, the properties of the holograms formed by a spherical particle that is illuminated by a plane wave or a shaped electromagnetic beam. Afterwards, the principle of the Debye series decomposition and the localization principle (LP) are employed to evaluate the contributions of the different scattering mechanisms. Section 3 briefly summarizes the basic steps of the code developed to perform these calculations as well the backpropagation of holograms. The paper concludes with section 4, where exemplifying numerical results are presented and discussed.

2 Exact calculation of hologram formation

2.1 Generalized Lorenz-Mie theory

A spherical particles, with radius a and refractive index m_p , is located in a continuous medium with refractive index m_0 . The particle is centered in the Cartesian coordinate system (Oxyz) and the spherical coordinate system (Or $\theta\phi$) where, classically, θ is the scattering angle [13]. The observation plane (O_pxyz_p), also referred as the hologram-recording plan (or CCD chip), is parallel to (xy) and distant of z_p from the particle centre. The particle, with relative refractive index $m_r = m_p / m_0$, is illuminated by an incident harmonic beam, with wavelength λ_0 and beam waist ω_0 , propagating along z . According to the GLMT [14, 15], the components of the electrical field vector $\mathbf{E}^s(\mathbf{r})$ that is scattered by the particle in the near or far-fields read as:

$$\begin{aligned} E_r^s &= -k_0 E_0 \sum_{n=1}^{+\infty} \sum_{m=-n}^{+n} c_n^{pw} A_n^m \begin{bmatrix} \xi_n''(k_0 r) \\ +\xi_n(k_0 r) \end{bmatrix} P_n^{(m)}(\cos\theta) e^{im\phi} \\ E_\theta^s &= -\frac{E_0}{r} \sum_{n=1}^{+\infty} \sum_{m=-n}^{+n} c_n^{pw} \begin{bmatrix} A_n^{m\xi'}(k_0 r) \tau_n^{(m)}(\cos\theta) \\ +m B_n^m \xi_n(k_0 r) \pi_n^{(m)}(\cos\theta) \end{bmatrix} e^{im\phi} \quad (1) \\ E_\phi^s &= -\frac{iE_0}{r} \sum_{n=1}^{+\infty} \sum_{m=-n}^{+n} c_n^{pw} \begin{bmatrix} m A_n^{m\xi'}(k_0 r) \tau_n^{(m)}(\cos\theta) \\ +B_n^m \xi_n(k_0 r) \tau_n^{(m)}(\cos\theta) \end{bmatrix} e^{im\phi} \end{aligned}$$

where (ξ_n, ξ'_n, ξ''_n) stand for Ricatti-Bessel functions and their derivatives, $k_0 = 2\pi/\lambda_0$ and E_0 for the wave vector and the amplitude of the incident beam at a particular point, c_n^{pw} is a coefficient specific to the plane wave illumination case with

$$c_n^{pw} = k_0^{-1} i^{n-1} (-1)^n (2n+1) / [n(n+1)] \quad (2)$$

The radial functions $P_n^{[m]}$, and $\tau_n^{[m]}, \pi_n^{[m]}$ are the associated Legendres polynomials and the generalized Legendres functions respectively,

$$P_n^{[m]}(\cos\theta) = (-1)^m (\sin\theta)^m \frac{d^m P_n(\cos\theta)}{(d\cos\theta)^m} \quad (3)$$

$$\tau_n^m(\cos\theta) = \frac{d}{d\theta} P_n^m(\cos\theta); \quad \pi_n^m(\cos\theta) = \frac{P_n^m(\cos\theta)}{\sin\theta}$$

where P_n and d stand for the Legendres polynomials of order n and the derivative operator respectively. The coefficients $A_n^m = g_{n, TM}^m a_n$ and $B_n^m = g_{n, TE}^m b_n$, where TM and TE stand for Transversal Magnetic (i.e. parallel polarization component) and Transversal Electric (i.e. perpendicular polarization component), are the generalized external scattering coefficients. They account for the particle shape *via* the external particle scattering coefficients a_n, b_n of the LMT, for homogeneous [13] (or multilayered [14]) spheres. The A_n^m and B_n^m also account for the beam shape through the beam shape coefficients (BSC) $g_{n, TM}^m, g_{n, TE}^m$ of the GLMT [15]. The integer numbers n and m stand for the expansion number of the LMT and the beam azimuth number of GLMT respectively. The analysis of the convergence of the infinite series (such as Eq. (1), or more simply a_n, b_n [13]) show that, after a slow oscillating behaviour, they converge rapidly when the value of n exceed the particle size parameter, ka . So that, the infinite series can be truncated and the limit $n \rightarrow +\infty$ replaced by a maximum value n_{max} estimated numerically with a fitting procedure. In the case of intermediate sized particles (i.e. $8 < ka < 4200$) [16], one can use:

$$n_{max} = k_0 a + \varepsilon_{max} (k_0 a)^{1/3} + 2 \quad (4)$$

with $\varepsilon_{max} = 4.05$. More details about the magnetic field and internal fields components as well as the different ways to calculate the BSC can be found in Refs. [14, 15].

2.2 Debye series and localization principle

From the expansion series of the LMT and the GLMT, little can be said about the particle scattering mechanisms. Debye series allow clarifying the situation by decomposing the series of the LMT in terms of partial waves that are meaningful in the frame of the more intuitive Geometrical Optics Approximation (GOA). For instance, the external scattering coefficient of a

homogeneous spherical particle maybe rearranged as follows:

$$\left. \begin{array}{l} a_{n,p} \\ b_{n,p} \end{array} \right\} = (1/2) \left[\left(1 - R_{n,\chi}^{(22)} \right) - T_{n,\chi}^{(21)} \left(R_{n,\chi}^{(11)} \right)^{p-1} T_{n,\chi}^{(12)} \right] \quad (5)$$

where $\chi = TE$ for a_n and $\chi = TM$ for b_n , p stands for the partial wave and scattering mechanism order (with $p=1$ for single refraction, $p=2$ for double refraction, etc.). The coefficients $R_{n,\chi}^{(22)}, R_{n,\chi}^{(11)}, T_{n,\chi}^{(21)}$ and $T_{n,\chi}^{(12)}$, whose expressions can be found in Ref. [17], correspond, respectively, to reflections of partial waves on the outer and the inner surface of the particle, and transmissions into and out of the particle. The external (as well the internal) scattering coefficients of the LMT can be retrieved from Debye series by summing all possible partial waves:

$$\left. \begin{array}{l} a_n \\ b_n \end{array} \right\} = (1/2) \left[1 - R_{n,\chi}^{(22)} - \sum_{p=1}^{+\infty} T_{n,\chi}^{(21)} \left(R_{n,\chi}^{(11)} \right)^{p-1} T_{n,\chi}^{(12)} \right] \quad (6)$$

Actually, in Eqs. (5) and (6), the last term into the brackets correspond to the different refracting processes ($p=1, 2, 3, \dots$, which intensity decrease rapidly for increasing p), while the first two terms, $(1 - R_{n,\chi}^{(22)})$, account for three scattering processes that are encompassed in the scattering order ($p=0$). The unit value is associated to a pure diffractive term [18, 19] since it is totally independent upon the particle material properties. In wave optics, it is this single term that it is generally assumed responsible for holograms formation. The second term, $R_{n,\chi}^{(22)}$ accounts for closely related scattering processes: surface waves, and grazing plus tunnelling rays. It is not possible to properly separate the later contributions in the frame of Debye series. However, this can be partly completed, approximatively, by invoking the localization principle (LP) introduced by Huslt's [8].

According to the LP, the expansion term n is also a partial wave number identifying rays (partial waves indeed) that hits or graze the particle surface at different distances ℓ_n from its centre

$$\ell_n = (n + 1/2) / k_0 \quad (7)$$

For $n + 1/2 = k_0 a$, this distance corresponds exactly to the particle radius a . The LP allows giving some meaning to Eq. (4). The first time ka corresponds to a region (from $n=1$ to $n \approx k_0 a$) where refracted and specular processes interact directly with the particle surface, while the second term $\varepsilon_{max} (k_0 a)^{1/3}$ corresponds to the width of a corona region surrounding the particle where grazing and tunnelling rays as well as surface wave effects take place [19]. The constant 2 is a fitting value ensuring a good convergence of the LMT series in a large variety of cases (i.e. particle size and refractive index ranges)[16].

3 Numerical calculation of hologram formation and backpropagation

The previous considerations have been implemented in a Matlab code allowing calculating accurately all the properties (amplitude, phase and intensity) of the incident, the internal, the scattered and the total electromagnetic field (incident plus scattered). The total electromagnetic intensity in the hologram-recording plane is simply a particular case. By using Debye series to calculate the external and internal scattering coefficients, the code allows separating the relative contributions (or calculate interference effects) of all refractive terms ($p=1,2,3\dots$) plus the pure diffractive term (contained in $p=0$). Then, the LP is used to truncate Debye's series in order to separate the grazing-plus-tunnelling contributions from the surface waves contributions. Particular attention has been paid to the numerical stability of the calculations for particles with a large size parameter. For the hologram back-propagation, the Fresnel or Rayleigh-Sommerfeld approximations are used as depicted in Ref. [4].

4 Results and discussion

The numerical results presented herein allows to highlight various features of the "Photonic Jet Method" that was introduced to estimate simultaneously the particle size, refractive index, 3D position and dynamics [4, 5, 7]. Fig. 1 (a) shows, from top to bottom, the direct calculation of the total electromagnetic intensity in the near-field and the (yz) plan, some contour lines of the unwrapped phase of the total electrical field, and the near-field intensity profile along the optical axis of an oil droplet in water. The latter, with radius $a=50\mu\text{m}$ and relative refractive index $m=1.0832$, is illuminated by a non-polarized plane wave with wavelength $\lambda=0.4753\mu\text{m}$. While Fig. 1 (a) accounts for all scattering processes (full LMT results), Fig. 1 (b-d) accounts only for (b) pure diffraction, (c) all non-diffractive terms included in the order ($p=0$), i.e. specular, grazing, tunnelling and surface waves and (d) for the single refraction ($p=1$). One can notice in Fig. 1 (a) the good agreement between LMT and Debye ($p=0,1,\dots,100$) results for the external as well as for the internal field. In Fig. 1 (b), the contribution of the non-diffractive components in the PJ region are clearly noticeable, when Fig. 1 (d) suggests that the structure of the caustic generated by refracted rays may be more complex that the one predicted by a GOA. The latter remarks are important for any attempt to develop a GOA or a Physical Optics Approximation (POA) of the PJ reconstruction.

Looking at the far field, it is again that the non-diffractive terms have a visible influence on the hologram characteristics, see Fig. 2. The parameters used for these simulations are identical to ones of the experimental setup of refs [5] (i.e. 4 megapixels camera located at 10 cm from a water droplet in air with diameter 1 mm, $\lambda=$

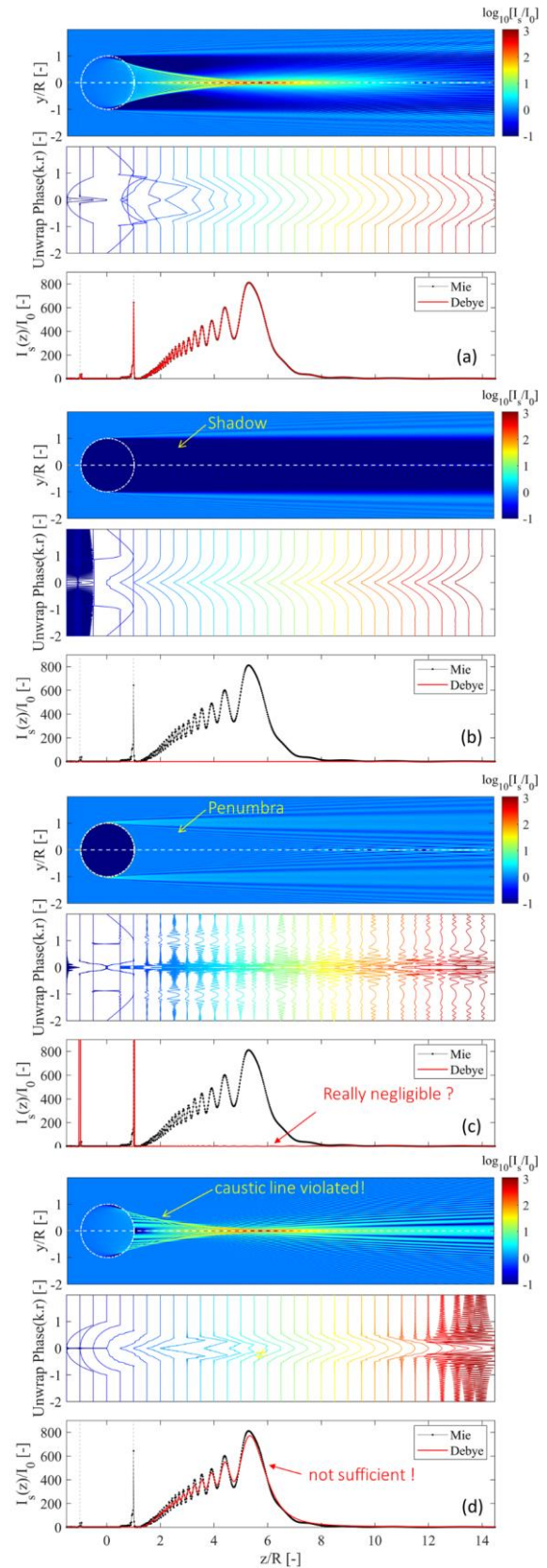


Figure 1 Near-field intensity map, unwrapped phase and axial-intensity profile when (a) all scattering process are included, (b) only pure diffraction, (c) only edge-wave contributions excluding pure diffraction and (d) only single refraction. Scatterer: oil droplet in water ($k_0a=661$).

0.633 μm). Fig. 3 shows the results obtained when two of these holograms (pure diffraction and single refraction) are back propagated. It is found that the differences are rather small between the axial intensity profiles of the PJ retrieved with the single term ($p=1$) and with full calculations. However, the contrast of the reconstructed PJ, regarding the surrounding background, appears rather noisy, suggesting that the single refractive term is not enough to fully describe the forward caustic region.

5 References

[1] J. W. Goodman, "Introduction to Fourier Optic," Mac. Graw-Hill, New York (1960).
 [2] S.-H. Lee, Y. Roichman, G.-R. Yi, S.-H. Kim, S.-M. Yang, A. v. Blaaderen, P. v. Oostrum, and D. G. Grier, "Characterizing and tracking single colloidal particles with video holographic microscopy," *Opt. Express* **15**, 18275-18282 (2007).
 [3] H. Shpaisman, B. J. Krishnatreya, and D. G. Grier, "Holographic microrefractometer," *Appl. Phys. Lett.* **101**, 091102 (2012).
 [4] M. P. L. Sentis, F. R. A. Onofri, and F. Lamadie, "Bubbles, drops, and solid particles recognition from real or virtual photonic jets reconstructed by digital in-line holography," *Opt. Lett.* **43**, 2945-2948 (2018).
 [5] M. P. L. Sentis, F. R. A. Onofri, and F. Lamadie, "Photonic jet reconstruction for particle refractive index measurement by digital in-line holography," *Opt. Express* **25**, 867-873 (2017).
 [6] L. Tian, H. Gao, and G. Barbastathis, "Digital holographic imaging of multi-phase flows," in *Imaging and Applied Optics*, OSA Technical Digest (CD) (Optical Society of America, 2011), CWB5.
 [7] M. P. L. Sentis, L. Bruel, S. Charton, F. R. A. Onofri, and F. Lamadie, "Digital in-line holography for the characterization of flowing particles in astigmatic optical systems," *Opt. Lasers Eng.* **88**, 184-196 (2017).
 [8] H. C. van de Hulst, *Light Scattering by Small Particles* (Dover Publications, New-York, 1957).
 [9] L. Yao, X. Wu, Y. Wu, J. Yang, X. Gao, L. Chen, G. Gréhan, and K. Cen, "Characterization of atomization and breakup of acoustically levitated drops with digital holography," *Appl. Opt.* **54**, A23-A31 (2015).
 [10] O. Kempainen, Y. Heinson, and M. Berg, "Quasi-three-dimensional particle imaging with digital holography," *Appl. Opt.* **56**, F53-F60 (2017).
 [11] F. Soulez, L. Denis, É. Thiébaud, C. Fournier, and C. Goepfert, "Inverse problem approach in particle digital holography: out-of-field particle detection made possible," *J. Opt. Soc. Am. A* **24**, 3708-3716 (2007).
 [12] T. Latychevskaia and H.-W. Fink, "Practical algorithms for simulation and reconstruction of digital in-line holograms," *Appl. Opt.* **54**, 2424-2434 (2015).
 [13] C. F. Bohren and D. R. Huffman, *Absorption and scattering of light by small particles* (Wiley & Sons, New York, 1998).
 [14] F. Onofri, G. Gréhan, and G. Gouesbet, "Electromagnetic scattering from a multilayered sphere located in an arbitrary beam," *Appl. Opt.* **34**, 7113-7124 (1995).
 [15] G. Gouesbet and G. Gréhan, *Generalized Lorenz-Mie Theories* (Springer, Berlin, 2011).
 [16] W. J. Wiscombe, "Improved Mie scattering algorithms," *Appl. Opt.* **19**, 1505-1509 (1980).
 [17] E. A. Hovenac and J. A. Lock, "Assessing the contribution of surface waves and complex rays to far-field scattering by use of the Debye series," *J. Opt. Soc. Am. A* **9**, 781-795 (1992).
 [18] H. M. Nussenzveig, "High-frequency scattering by an impenetrable sphere," *Annals of Physics* **34**, 23-95 (1965).

[19] J. A. Lock and P. Laven, "Mie scattering in the time domain. Part II. The role of diffraction," *J. Opt. Soc. Am. A* **28**, 1096-1106 (2011).

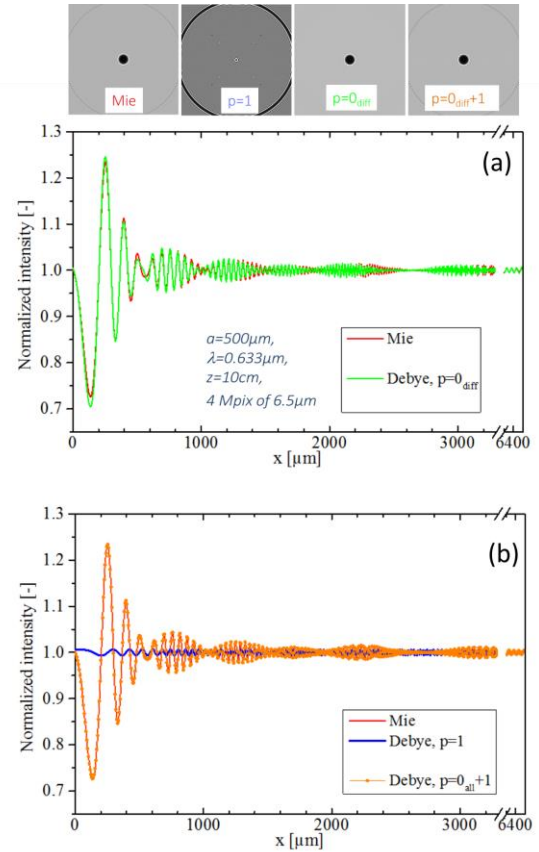


Figure 2 Holograms (gray images) and their radial intensity profiles when all scattering processes are taken into account (Mie), only pure diffraction ($p=0_{diff}$), only single refraction ($p=1$), single refraction and reflections ($p=0_{all+1}$). Water droplet in air ($ka=4963$).

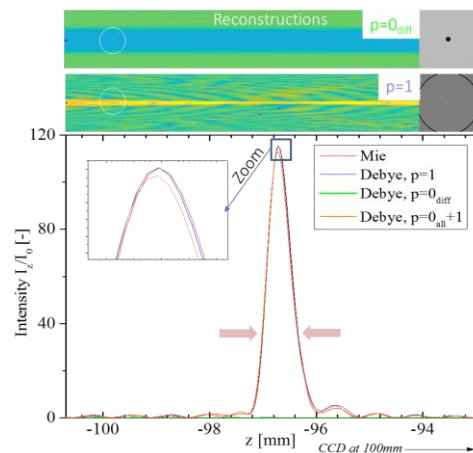


Figure 3 Backpropagation of holograms of Fig. 2 and corresponding axial intensity profiles in the PJ region.